

AD-A116 861

SCIENTIFIC RESEARCH ASSOCIATES INC GLASTONBURY CT F/G 20/12
THREE-DIMENSIONAL NUMERICAL STUDIES OF THE PHYSICS OF SEMICONDU—ETC(U)
JUL 82 N S LIU, S J SHAMROTH, H L GRUBIN N00014-82-C-0140
UNCLASSIFIED SRA-R82-920013-4 ML

1 of 1
A &
10-101



AD A116861

DTIC FILE COPY

Unclassified

SECURITY CLASSIFICATION OF THIS PAGE (When Data Entered)

12

REPORT DOCUMENTATION PAGE		READ INSTRUCTIONS BEFORE COMPLETING FORM
1. REPORT NUMBER R82-920013-4	2. GOVT ACCESSION NO.	3. RECIPIENT'S CATALOG NUMBER
4. TITLE (and Subtitle) Three-Dimensional Numerical Studies of the Physics of Semiconductor Crystal Growth		5. TYPE OF REPORT & PERIOD COVERED Final Report 1 Jan - 30 June 1982
7. AUTHOR(s) N.S. Liu S.J. Shamroth H.L. Grubin		6. PERFORMING ORG. REPORT NUMBER
9. PERFORMING ORGANIZATION NAME AND ADDRESS Scientific Research Associates, Inc. P.O. Box 498 Glastonbury, CT 06033		8. CONTRACT OR GRANT NUMBER(s) N00014-82-C-0140
11. CONTROLLING OFFICE NAME AND ADDRESS Office of Naval Research Department of the Navy 800 N. Quincy St., Arlington, VA 22217		10. PROGRAM ELEMENT, PROJECT, TASK AREA & WORK UNIT NUMBERS
14. MONITORING AGENCY NAME & ADDRESS (if different from Controlling Office) DCASMA- Hartford 96 Murphy Road Hartford, CT 06114		12. REPORT DATE July 1982
		13. NUMBER OF PAGES 40
		15. SECURITY CLASS. (of this report) Unclassified
		15a. DECLASSIFICATION/DOWNGRADING SCHEDULE
16. DISTRIBUTION STATEMENT (of this Report) Approved for public release; distribution unlimited		
17. DISTRIBUTION STATEMENT (of the abstract entered in Block 20, if different from Report)		
18. SUPPLEMENTARY NOTES		
19. KEY WORDS (Continue on reverse side if necessary and identify by block number) Hydrodynamic equations, Czochralski crystal growth, semiconductors, melt patterns		
20. ABSTRACT (Continue on reverse side if necessary and identify by block number) Three-dimensional numerical computational fluid dynamics are used to show the feasibility of simulating Czochralski crystal growth under nonideal growing conditions.		

DD FORM 1 JAN 73 1473

EDITION OF 1 NOV 65 IS OBSOLETE

Unclassified

SECURITY CLASSIFICATION OF THIS PAGE (When Data Entered)

Report R82-920013-4
Contract N00014-82-C-0140

Three-Dimensional Numerical Studies of the
Physics of Semiconductor Crystal Growth

N.S. Liu
S.J. Shamroth
H.L. Grubin

Scientific Research Associates, Inc.
P.O. Box 498
Glastonbury, CT 06033

July 1982

DESAT Phase I

Final Report for Period 1 January 1982 - 30 June 1982

TABLE OF CONTENTS

Page

INTRODUCTION.	1
PHASE I TECHNICAL OBJECTIVES.	3
NUMERICAL CONSIDERATIONS.	4
ANALYSIS.	7
RESULTS	11
THREE-DIMENSIONAL CALCULATION	15
CONCLUSIONS	17
REFERENCES.	18
FIGURES	19
APPENDIX.	36



Accession For	
NTIS GRA&I	<input checked="checked" type="checkbox"/>
DIC TAP	<input type="checkbox"/>
Unannounced	<input type="checkbox"/>
Justification	
By _____	
Distribution/	
Availability Codes	
Full and/or	
Dist	Special
A	

1. INTRODUCTION

It is axiomatic that all phases of future semiconductor device development, such as that indicated by the VLSI (very large scale integration), and VHSIC (very high speed integrated circuits) programs depend on the quality of the semiconductor material. Growers of these materials, e.g., silicon, gallium arsenide, and indium phosphide, etc., are interested in efficient, reliable methods that yield defect-free and dislocation-free semiconductors. Over many years, a variety of different techniques have been developed to grow materials, some overcoming disadvantages or shortcomings of earlier methods, while others are designed to overcome specific problems associated with the growth of a particular semiconductor. Examples here include the Czochralski pull method which was developed, among other reasons, to minimize temperature variations in the melt. The Czochralski method is one of the most common crystal growing techniques used in silicon technology and single crystals three or four inches in diameter are common today. Another example involves a modification of the Czochralski method and incorporates liquid encapsulation. This is finding increased use in gallium arsenide technology, where it tends to eliminate arsenic in the growth system. The development and use of these growth systems and others (e.g., Bridgeman, zone refining, floating zone, vapor, liquid and molecular beam epitaxy, chemical vapor deposition, etc.), has been largely empirical due in a major part to the absence of physical theories with predictive capabilities. These difficulties lie in two groups. The first involves the incomplete picture of growth mechanisms. The second, while interrelated to the first, recognizes the fact that growth is fundamentally a three-dimensional phenomena and that one- or two-dimensional theoretical approximations of this phenomena will not necessarily predict in a meaningful way such things as the local temperature distribution near the solid-liquid interface, temperature distributions within the melt due to heating coils, the distribution of unwanted impurities arising from contamination by the crucible, etc.

The question then becomes: How can one successfully undertake a program that attempts to simulate crystal growth and thereby provide a basic physics for this growth. An attempt as a partial answer to this question is the subject of this report which summarizes Scientific Research Associates Phase I DESAT

study for simulating Gochralski crystal growth. The Phase I study relied strongly on the attitude that fluid flow in the melt is one of the major influences on the final properties of the grown crystal [Refs. 1-10]. As a consequence, it dealt solely with obtaining solution to the relevant hydrodynamic equations for examining flow patterns in the melt.

2. PHASE I TECHNICAL OBJECTIVES

✓
The primary purpose of the Phase I study was to establish the feasibility of developing reliable theories with predictive capability in the area of crystal growth. Within the guidelines of the DESAT program the proposed study was limited to an area where some computational fluid dynamic studies have already appeared and where numerous experimental results have been reported; namely, the area of Czochralski crystal pulling. The intent of the study was to generalize all previously developed work, and to incorporate three-dimensional effects, which invariably arise when stirring is included. For Czochralski growth nonaxisymmetric effects were formulated and numerical simulations were performed for two cases: (1) a local hot spot on the crucible wall, and (2) angular misalignment between the crystal and crucible rotational axes. ↗

3. NUMERICAL CONSIDERATIONS

In the Czochralski method of crystal growth, the growing crystal is pulled slowly from the center of a rotating crucible of melt material and the resultant crystal properties are strongly influenced by details of the melt thermal and velocity fields. The melt flow represents a relatively complex fluid mechanics phenomenon. As shown in the schematic of Fig. 1, the melt is contained in a nominally axisymmetric crucible of constant temperature which may be rotating about its axis. The crystal which develops at the melt upper surface is nominally concentric with the crucible and both axes are nominally aligned. The crystal rotates about its axis during the growth process. The upper surface of the melt is a free surface whose shape is determined by the constant pressure free surface boundary condition and a meniscus of unknown shape occurs at the melt-crystal boundary. Heat transfer at the melt-crystal boundary is determined by heat conduction away from this boundary within the crystal and the heat transfer at the melt free surface is determined by radiative effects to the atmosphere. Finally, the melt motion is driven both by inertial and viscous forces associated with the crystal and crucible rotation and by bouyancy forces arising due to temperature differences within the melt. Obviously, with all these phenomena affecting the flow, a prediction of the melt velocity and temperature fields is a formidable task.

To date, several investigations have focused upon predictions of the melt flow field. In a relatively early work Kobyashi and Arizumi (Ref. 2) considered axisymmetric flow situations and solved the steady-state stream function-vorticity form of the Navier-Stokes equations in the melt and a heat conduction equation in the crystal to determine the shape of the crystal-melt interface. The analysis included the effects of bouyancy, but assumed the melt free surface to be flat. Using a numerical over-relaxation technique to solve the equations, the authors obtained converged solutions and examined the effects of fluid motion on the interface shape for viscous bulk Czochralski flows.

In a more recent effort Langlois and Shir (Ref. 6) applied the unsteady Navier-Stokes equations (again in stream function - vorticity form) to the melt flow field problem. As in Ref. 2, the melt free surface was assumed to be flat; however, since the generated flow field was the item of primary interest in this study, the interface surface was also assumed flat. The equations were solved by using an explicit time marching procedure for the vorticity equation and a successive over-relaxation procedure (SOR) for the stream function equation at each time step. Steady state solutions were obtained to show the effect of bouyancy on the flow field for several demonstration test cases at physically unrealistic low Reynolds numbers (high viscosities or small crucibles).

The Langlois-Shir effort of Ref. 6 was extended by Langlois in Ref. 7 to cases having realistic Reynolds numbers. Several cases were considered, and the cases run included bouyancy effects, isothermal flows, stationary crucibles, rotating crucibles and effect of viscosity variation. The calculations were run using the numerical method described in Ref. 6 and for the cases considered this method required a very large amount of computer run time. According to Langlois, each case of Ref. 7 required twenty-five (25) minutes of IBM 360/195 computation time per simulated physical second. Since the isothermal case with rotating crucible was run for more than thirty-five (35) simulated seconds, this case required over fourteen (14) hours of run time. For the case of a stationary crucible, a steady state was reached in an uneventful manner. However, when the crucible was rotated in addition to the crystal, the secondary flow switched between two distinct patterns. In general, the results obtained seemed physically reasonable. More recent studies by Langlois appear in Refs. 8 and 9.

The approaches of Refs. 2, 6-9 demonstrate the ability of computational methods to impact upon the melt velocity and thermal field predictions. However, these efforts were confined to axisymmetric flow and, therefore, could not assess possible three-dimensional effects on the crystal growth process. Although the physical problem is nominally axisymmetric, possible sources of three-dimensional effects are temperature hot spots on the crucible wall, impurities entering the melt from the crucible, non-axisymmetric crucible or crystal geometries, misalignment of the crystal and crucible axes, misalignment of the axes from the vertical, etc. Even when no such three-dimensional "forcing functions" are present, it is possible that three-dimensional flow patterns may occur due to hydrodynamic instabilities

(e.g. see Ref. 11). Hence, the three-dimensional aspects of the problem may have significant impact on the crystal growth process.

Although the stream function - vorticity formulation of Refs. 2, 6-9 could be extended to three-dimensional flow in principle, in practice the three-dimensional stream function vorticity approach is difficult, cumbersome and in general has not been used in solving three-dimensional hydrodynamic problems. A much more straight-forward and efficient approach would be based upon a solution of the Navier-Stokes equations with primitive variables, velocity and pressure (or density), used as dependent variables. Such an approach is used here to demonstrate a model three-dimensional melt flow field calculation.

In addition to its advantage in a straight-forward application to three-dimensional melt flow field problems, the velocity-pressure approach also allows a more direct analysis to the free surface condition. If the free surface is to be properly modeled, it is necessary to apply a pressure boundary condition there, and as pointed out by Langlois (Ref. 6), application of this pressure boundary condition in the stream function-vorticity framework may be difficult. When primitive variables are used, application of the free surface boundary condition is expected to be considerably easier.

4. ANALYSIS

The crystal growth melt problem focuses upon thermal and velocity fields of a nearly incompressible fluid driven by inertial, viscous and bouyancy forces. The bouyancy forces result from fluid temperature variation causing a slight density variation which leads to a gravitational body force. The present approach uses the Boussinesq type approximation in which the buoyancy force is modelled as a body force proportional to the difference between the local temperature and a reference temperature. This approach has been used in Refs. 2, 6-9 and its validity requires changes in temperature to be small compared to the mean temperature. Therefore, the relevant equations to be solved are the incompressible Navier-Stokes equations with bouyancy represented by a body force dependent upon the local temperature.

The present effort has several aims including the demonstration of a three-dimensional calculation capability and development of an efficient computer code. A numerical solution procedure which has proven to be efficient in a wide range of fluid mechanics problems is the linearized block implicit (LBI) procedure of Briley and McDonald (Refs. 12 and 13). Since the procedure has been described in considerable detail elsewhere, it shall only be briefly outlined here. The reader interested in greater detail should refer to [12,13]. The method can be briefly outlined as follows: the governing equations are replaced by an implicit time difference approximation, optionally a backward difference or Crank-Nicolson scheme. Terms involving nonlinearities at the implicit time level are linearized by Taylor expansion in time about the solution at the known time level, and spatial difference approximations are introduced. The result is a system of multidimensional coupled (but linear) difference equations for the dependent variables at the unknown or implicit time level. To solve these difference equations, the Douglas-Gunn [14] procedure for generating alternating-direction implicit (ADI) schemes as perturbations of fundamental implicit difference schemes is introduced. This technique leads to systems of coupled linear difference equations having narrow block-banded matrix structures which can be solved efficiently by standard block-elimination methods.

The method centers around the use of a formal linearization technique adapted for the integration of initial-value problems. The linearization technique, which requires an implicit solution procedure, permits the solution of coupled nonlinear equations in one space dimension (to the requisite degree of accuracy) by a one-step noniterative scheme. Since no iteration is required to compute the solution for a single time step, and since only moderate effort is required for solution of the implicit difference equations, the method is computationally efficient; this efficiency is retained for multidimensional problems by using ADI techniques. The method is also economical in terms of computer storage, in its present form requiring only two time-levels of storage for each dependent variable. Furthermore, the ADI technique reduces multidimensional problems to sequences of calculations which are one dimensional in the sense that easily-solved narrow block-banded matrices associated with one-dimensional rows of grid points are produced.

One immediate problem which arises in the application of the LBI procedure to incompressible problems is the lack of a time derivative of pressure appearing in the governing equations. As shown by Briley and McDonald, the LBI approach requires the appearance of time derivatives of each dependent variable. Therefore, if this procedure is to be used, a device of some sort must be created to introduce the missing time derivative into the equations. One method of treating this problem is the so-called artificial compressibility approach in which a time-derivative of the required variable (e.g. pressure) is introduced into the set of equations, and the equations are marched to steady state. When steady state is reached, the time derivative is zero and the solution satisfies the required steady state equations. Such an approach has been used by several investigators e.g. Chorin (Ref. 15).

The present approach utilizes a similar philosophy in a somewhat different context and is based upon the analysis of Briley, McDonald and Shamroth which shows that for constant total temperature flow, the compressible flow equations reduce to the incompressible equations as the Mach number approaches zero. This analysis has been derived in an internal SRA report which is included as an Appendix of the present report. Following this analysis, the present approach approximates the governing equations by a set of low Mach number compressible flow equations and a gas law consistent with a constant total temperature flow. It should be noted that the constant total temperature

assumption is only incorporated into the assumed gas law thus making the equations of continuity and momentum approximate the incompressible flow equations. The momentum equation contains a body force type term representing buoyancy which depends upon local physical temperature and the local temperature is determined from an energy equation.

With this introductory paragraph in mind, the equations used are the momentum equation,

$$\rho \left[\frac{\partial \mathbf{V}}{\partial t} + (\mathbf{V} \cdot \nabla) \mathbf{V} \right] = -\nabla P + \mathbf{F} - \nabla \times [\mu(\nabla \times \mathbf{V})] + \nabla[(\frac{1}{3}\mu)\nabla \cdot \mathbf{V}] \quad (1)$$

the continuity equation,

$$\frac{\partial \rho}{\partial t} + \nabla \cdot (\rho \mathbf{V}) = 0 \quad (2)$$

and the energy equation

$$\rho \left[\frac{De}{Dt} + P \frac{D}{Dt} \left(\frac{1}{\rho} \right) \right] = \frac{\partial Q}{\partial t} + \Phi + \kappa \nabla^2 T \quad (3)$$

where t represents time, ρ represents density, P represents pressure, \vec{V} represents velocity, \vec{F} represents body force, μ represents viscosity, e represents internal energy, Q represents internal heat generation, κ represents thermal conductivity and Φ is the viscous dissipation function (which is a function of velocity derivatives). D/Dt represents the material or Stokes derivative. These equations must be supplemented by an equation of state which in general relates ρ , p and T ; and expressions which relate viscosity and thermal conductivity to temperature.

In regard to the equation of state, the analysis (see Appendix) shows that a constant total temperature fluid approaches an incompressible behavior as the Mach number approaches zero. Therefore, the equation of state is taken as

$$P = \rho R \left(\tau - \frac{V^2}{2C_p} \right) \quad (4)$$

where R is the gas constant and C_p is specific heat. If τ were the local total temperature in the fluid, Eq. (4) would represent the perfect gas law for an ideal fluid. However, in the present case τ is taken as a fictitious constant temperature of high enough value so that the Mach number, M_τ based

upon V and τ is small; i.e.,

$$M_r = |V| / \sqrt{\gamma R (\tau - V^2/2C_p)} \ll 1.0$$

In the present calculations this Mach number was kept below 0.03 and consequently the equations approach their incompressible form. The final item to be considered is the bouyancy force. In the present calculations, the bouyancy force is represented by the Boussinesq relation

$$\bar{F} = +\rho \bar{g} \beta (T - T_r) \quad (5)$$

where β is the volumetric coefficient of expansion, g is the acceleration due to gravity, T is the local temperature and T_r is a reference temperature.

The boundary conditions used in the present analysis consist of no-slip and one-sided momentum equations on all solid surfaces. On the free surface, the velocity normal to the surface is zero, the normal derivatives of the other velocity components are zero and a one-sided momentum equation is solved. The temperature is specified on both the crystal and crucible surfaces and a second normal derivative of temperature is set to zero on the free surface. The equations are solved as a coupled system with convergence acceleration techniques of the type described by McDonald and Briley (Ref. 16).

5. RESULTS

Several calculations were run under the present effort. These included a code verification test case, axisymmetric cases with and without bouyancy effects and a three-dimensional demonstration case. These are now discussed in detail.

The first case was run to verify the code against a known analytic solution. The case considered was flow within a rotating crucible with no crystal in the free surface. For this case the analytic solution for the azimuthal velocity component is

$$V_{\theta}(r) = V_w \frac{r}{r_w}$$

where V_w is the velocity at the wall and r_w is the wall radius. The calculation was run by assuming an initial flow and marching the equations in time until convergence was obtained. Convergence was judged by monitoring the maximum flow field residual as well as the maximum change in dependent variables over a time step. A comparison between the predicted V_{θ} profile and that obtained from the analytic solution for an incompressible fluid is given in Table I. As can be seen, the numerical solution is in excellent agreement with analysis. The calculation was repeated for flow between co-rotating cylinders and the comparison between the numerical predictions and the known analytic solution again was very good. These comparisons serve to verify the code for these simple test cases.

The second case considered was axisymmetric flow in a stationary crucible with the crystal rotating. If the crystal radius is denoted by R_1 , the crucible

r	V_{θ}	
	Predicted	Analytical
1.0	1.000	1.0
.95	.9499	.95
.90	.8999	.90
.85	.8499	.85
.80	.7999	.80
.75	.7499	.75
.70	.6989	.70
.65	.6499	.65
.60	.5988	.60
.55	.5498	.55
.50	.4998	.50
.45	.4498	.45
.40	.3998	.40
.35	.3498	.35
.30	.2998	.30
.25	.2499	.25
.20	.1999	.20
.15	.1499	.15
.10	.0999	.10
.05	.0499	.05
.0	.0	.0

Table I - Comparison of predicted and analytical velocity profiles for rotating crucibles

radius by R_2 , the crystal azimuthal velocity at R_1 by V_1 , the crucible azimuthal velocity by V_2 , the crucible height by h and the viscosity by ν , then the relevant problem parameters were

$$R_2/R_1 = 1.5$$

$$V_2/V_1 = 0.$$

$$Re = \frac{V_1 R_1}{\nu} = 4036$$

$$h/R_1 = 0.94$$

The Reynolds number Re represents the ratio of inertial to viscous forces and this value represents a typical crystal growth process in which $R_1 = 4.2\text{cm}$, $R_2 = 6.4\text{cm}$, $V_1 = 9.7\text{cm/sec}$, $V_2 = 0 \rightarrow 10\text{cm/sec}$, $h = 3.95\text{cm}$ and $\nu = 0.01\text{cm}^2/\text{sec}$. Bouyancy effects were set to zero for this case. With these parameters the case corresponds to the stationary crucible case considered by Langlois in Ref. 6.

The calculation run on a grid containing thirty-one (31) radial points and twenty-seven (27) axial points converged to a steady solution within eighty (80) time steps. The present deck is a very general code designed for maximum flexibility in which equations, dependent variables, grid specification, boundary conditions, etc. can be easily changed and, therefore, the code contains a great deal of computer overhead. Even with this large amount of overhead, the code required less than five (5) seconds of CDC 7600 time per time step. Recent changes designed to decrease run time (accompanied by a decrease in code flexibility) have decreased run time by a factor of 2. If the calculation were repeated with this new code, the total run time would be approximately 3 minutes. It is anticipated that further streamlining of the code will reduce run time by an additional factor of 3.

Predictions of the velocity and temperature fields are shown in Figs. 2-4. Both the Langlois calculation and the present calculation reached a steady state. The azimuthal velocity, Fig. 2, shows good qualitative agreement with the Langlois solution. Both calculations show the thin boundary layer on the crystal face as well as the local maximum near the stationary crucible wall. The predicted secondary flow field (Figure 3) shows the velocity components $V_z + V_r$ and is also in good qualitative agreement with the results of Langlois. Both calculations show the secondary flow to consist of a single

vortex pattern which is centered in the upper right corner of the flow field. Finally, temperature contours are shown in Fig. 4 where the ratio of the crucible wall temperature to the crystal face temperature is 1.052.

The next case considered corresponds to Langlois rotating crucible case without buoyancy forces. The parameters were now changed so that

$$V_2/V_1 = -1.02$$

All other parameters correspond to that of the first case and again buoyancy is neglected. When buoyancy is neglected the velocity field is unaffected by the thermal field and hence the resulting velocity field represents an isothermal calculation. The calculation was again run on a 31×27 computational grid, however, in this case complete convergence was not obtained. The major region of oscillation occurred near the free surface at radii just beyond the crystal boundary, (R_1). The velocity in this region was not well resolved and it is likely that this lack of resolution may have prevented convergence. However, the calculation did not show the unsteady flow pattern observed in Langlois case where the secondary flow shifted between two distinct patterns.

The azimuthal velocity contours for this case are shown in Fig. 5. The contours show the Taylor column under the crystal face and are in good qualitative agreement with the results of Langlois. The four different regions within the Taylor column discussed by Langlois are clearly evident. Directly under the crystal fluid turns with the crystals rather than with the crucible. This is followed by a transition region in which the flow azimuthal velocity changes from the crystal to the crucible direction. Next comes a region where the velocity changes little with depth and finally the boundary region at the crucible bottom.

The secondary flow vector plot in Fig. 6 shows four distinct vortices: a strong clockwise vortex just under the crystal face, a large but weaker counterclockwise vortex encompassing most of the region between the first vortex and the crucible bottom and two weak vortices in the outer radial region. These latter two vortices are very much elongated in the z -direction. Langlois' solution showed a weak vortex in the outer region which shifted between two patterns. The maximum values of the predicted-secondary flow velocities are approximately $0.10 V_1$ within the Taylor column and $0.02 V_1$ outside of the Taylor column.

These values are in good agreement with those given by Langlois. Temperature profiles are presented in Fig. 7.

The final axisymmetric case considered adds bouyancy effects to the calculation. The flow parameters used were those of the proceeding case with the following additions

$$P_r = 0.08$$

$$\frac{g}{\beta_r} (T_{\text{crucible}} - T_{\text{crystal}}) = 1.0$$

The results are presented in Figs. 8-10. The azimuthal velocity field shown in Fig. 8 again is in qualitative agreement with Langlois' calculation. In particular the change due to bouyancy effects (see Figs. 5 and 8) correspond to the changes shown by Langlois. The most dramatic change due to bouyancy occurs in the secondary flow profile where as shown in Fig. 9, the strength of the secondary flow pattern is increased considerably. The temperature field in this case shown in Fig. 10. These also show good qualitative agreement with Langlois.

6. THREE DIMENSIONAL CALCULATION

The final calculation focused upon three dimensional effects. Before discussing this calculation several points should be considered. First of all, three-dimensional calculations make major demands on computer resources and, therefore, for this demonstration calculation a flow field was chosen to allow the calculation to be made with a moderate number of grid points (an 11 x 17 x 16 grid was used). This relatively small number of three-dimensional grid points required the Reynolds number to be smaller than would normally be expected in a physical problem. Therefore, the case must be viewed as a demonstration case.

The second point concerns the source of the three dimensionality. It was originally anticipated that the three dimensionality would result from the angular misalignment of the crystal and crucible. The present effort assumes a flat free surface and, therefore, the effect of angular misalignment would be confined to changing the region on the upper surface bounded by the crystal from a circle to an ellipse. For a 5-degree misalignment, the resulting ellipse would have a ratio of major to minor axis of 1.004. In the absence of meniscus effects, the three dimensionality arising from misalignment would be negligible and, therefore, a second three dimensional source arising from a hot spot on the crucible wall was added to the calculation.

The calculation was run using 16 radial grid points, 11 axial grid points and 17 azimuthal grid points. The crystal was assumed to be rotating and the crucible stationary.

The geometrical parameters were taken as

$$R_2/R_1 = 1.5$$

$$h/R_1 = 0.5$$

The flow parameters were taken as

$$Re = V_1 R_1 / \nu = 100$$

$$P_r = .05$$

$$\frac{\beta}{Fr} (T_{crucible} - T_{crystal}) = .02$$

where V_1 is the velocity at the crystal radius, R_1 , ν is viscosity, P_r is Prandtl number, β is the volumetric coefficient of expansion and Fr is the Froude number. The ratio of the crucible wall temperature to the crystal

temperature was taken to be 1.052 and the hot spot temperature ratio was taken as 1.157. In order to further limit the computational domain two identical hot spots were assumed present. These were centered at $z/h = 0.4$, $\theta = \pi/2$ and $z/h = 0.4$, $\theta = 3\pi/2$. This specification allowed the calculation to be confined to the domain $0 < \theta < \pi$.

The calculation was first converged as an axisymmetric calculation with no axis angular misalignment and constant crucible wall temperature. The azimuthal velocity contours, secondary flow vector plots and temperature contours are shown in Figs. 11-13. The results are as expected with the low Reynolds number allowing significant azimuthal velocity to occur through most of the flow field (compare this to Fig. 2 where $Re = 4000$). A wall hot spot was then added to the problem and a three-dimensional calculation initiated from the converged two-dimensional calculations. Although both the velocity and temperature fields showed a three-dimensional variation, the velocity field variation in the azimuthal direction was very small. Both the azimuthal velocity contours and secondary flow pattern corresponded very closely to the axisymmetric case. The temperature field showed significant variation and the temperature field in various azimuthal planes are shown in Figs. 14-16. The calculation then was continued with a 5-degree angular misalignment between the crystal and crucible axes; as previously discussed, the addition of this misalignment factor was not large enough to change the predicted flow field.

7. CONCLUSIONS

The present effort has applied a Navier-Stokes analysis using velocity and density as dependent variables to the crystal growth melt problem.. The approach models the equations governing the velocity field as low Mach number compressible flow equations with a body force proportional to the local temperature and a gas law which approximates incompressible flow. The analysis has been applied to flow within a rotating cylinder and flow between two concentric cylinders, and in both cases the predicted azimuthal velocity field showed excellent agreement with the analytic solution to the governing equations. Axisymmetric melt problems which included the effects of bouyancy and crucible rotation were run and the predicted velocity and thermal fields showed good qualitative agreement with the vorticity-stream function solutions of Langlois. The approach was then applied to a model three-dimensional problem in which the three dimensionality resulted from a hot spot on the crucible wall. Although the flow parameters (particularly the low Reynolds number) required this to be viewed as a model calculation, the calculation definitely showed the capability of the procedure to calculate three-dimensional flows. An assessment of the effects of three-dimensional sources upon the crystal growth process will require further code evaluation; code 'speed-up' and extension of the code to include items such as the free surface boundary.

8. REFERENCES

1. Runyan, W. R.: Silicon Semiconductor Technology, McGraw-Hill Book Company (1965).
2. Kobayashi, N. and Arizumi, T.: Jap. J. App. Phys., 9, 361 (1970).
3. Kobayashi, N. and Arizumi, T.: Jap. J. App. Phys., 9, 1255 (1970).
4. Kobayashi, N.: J. Crystal Growth, 52, 425 (1981).
5. Carruthers, J.R. and Nassau, K.: J. App. Phys., 39, 5205 (1968).
6. Langlois, W.E. and Shir, C.C.: Comp. Meth. in App. Mech. and Eng., 12, 145 (1977).
7. Langlois, W.E.: J. Crystal Growth, 42, 386 (1977).
8. Langlois, W.E.: J. Crystal Growth, 46, 743 (1979).
9. Langlois, W.E.: J. Crystal Growth, 48, 25 (1980).
10. Mihelcic, M., et al: J. Crystal Growth, 53, 337 (1981).
11. Greenspan, H.P.: The Theory of Rotating Fluids, Cambridge University Press (1970).
12. Briley, W.R. and McDonald, H.: J. Comp. Phys., 24, 372 (1977).
13. Briley, W.R. and McDonald, H.: J. Comp. Phys., 34, 54 (1980).
14. Douglas, J. and Gunn, J.E.: Numerische Math., 6, 428 (1964).
15. Chorin, A.J.: Math. Comp. 22, 745 (1968).
16. McDonald, H. and Briley, W.R.: AIAA Paper 79-1495 (1979).

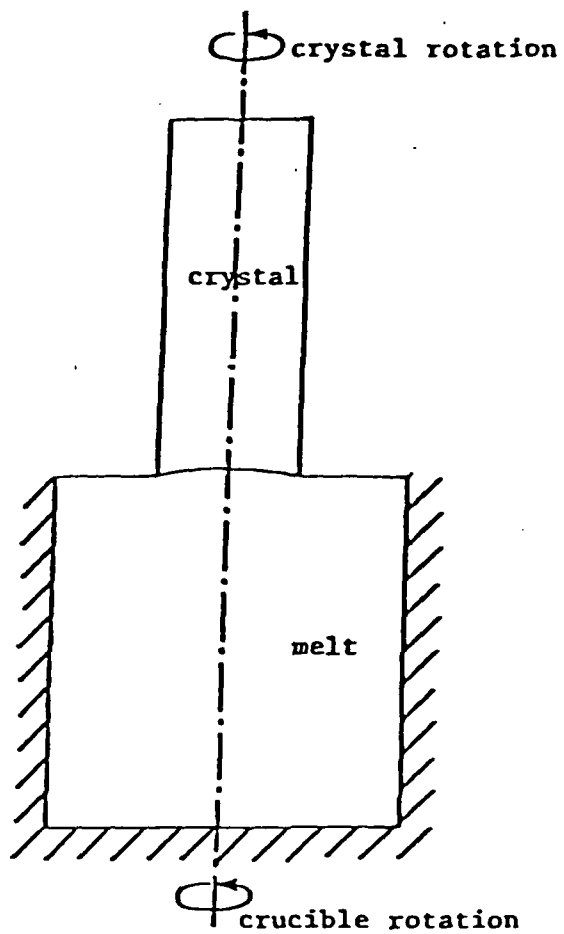


Fig. 1a - Axisymmetric Czochralski growth.

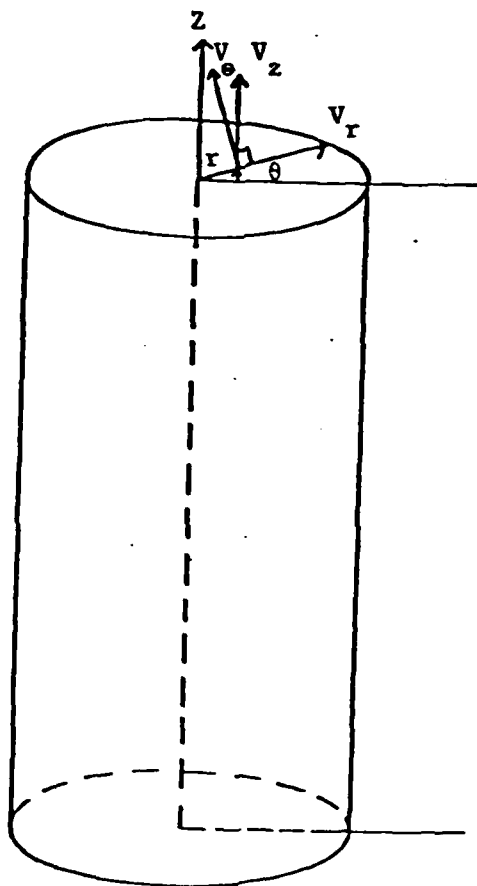


Fig. 1b - The cylindrical coordinates system and the velocity components.

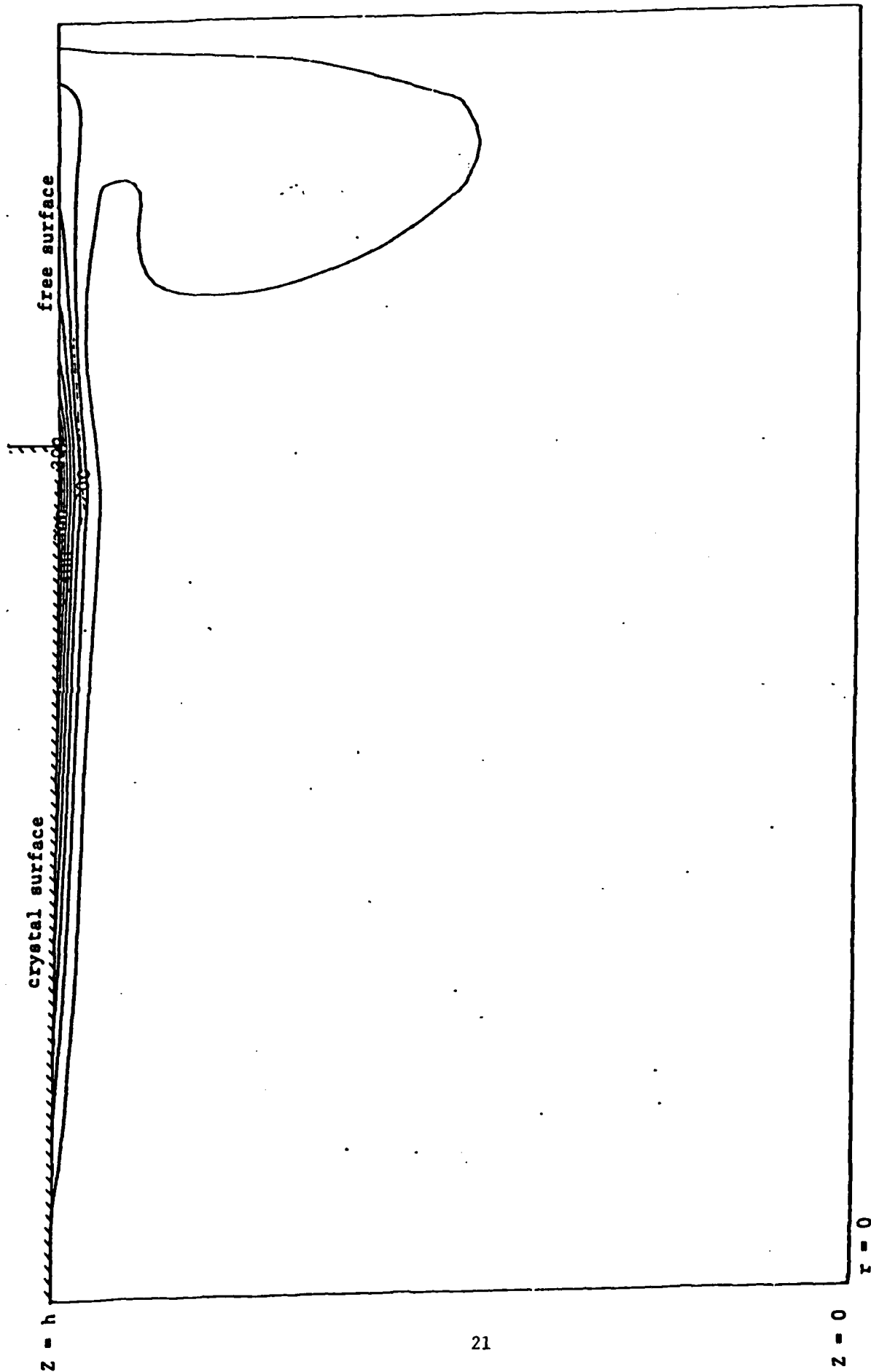


Fig. 2 - Azimuthal velocity contours, stationary crucible case. Contour levels at $-0.9, -0.8, -0.7, -0.6, -0.5, -0.4, -0.3, -0.2, -0.1$.

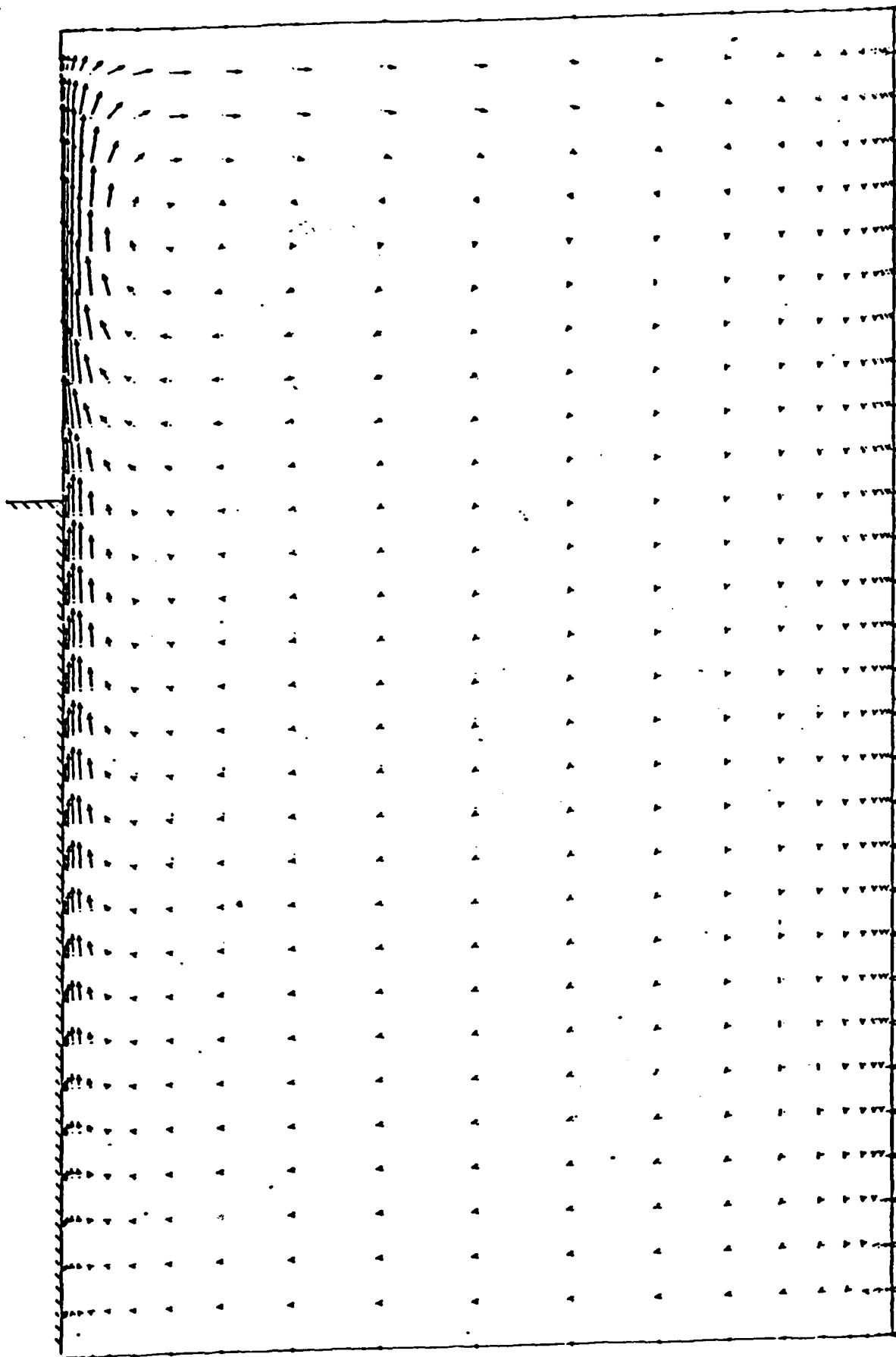


Fig. 3 - Secondary flow, stationary crucible case.

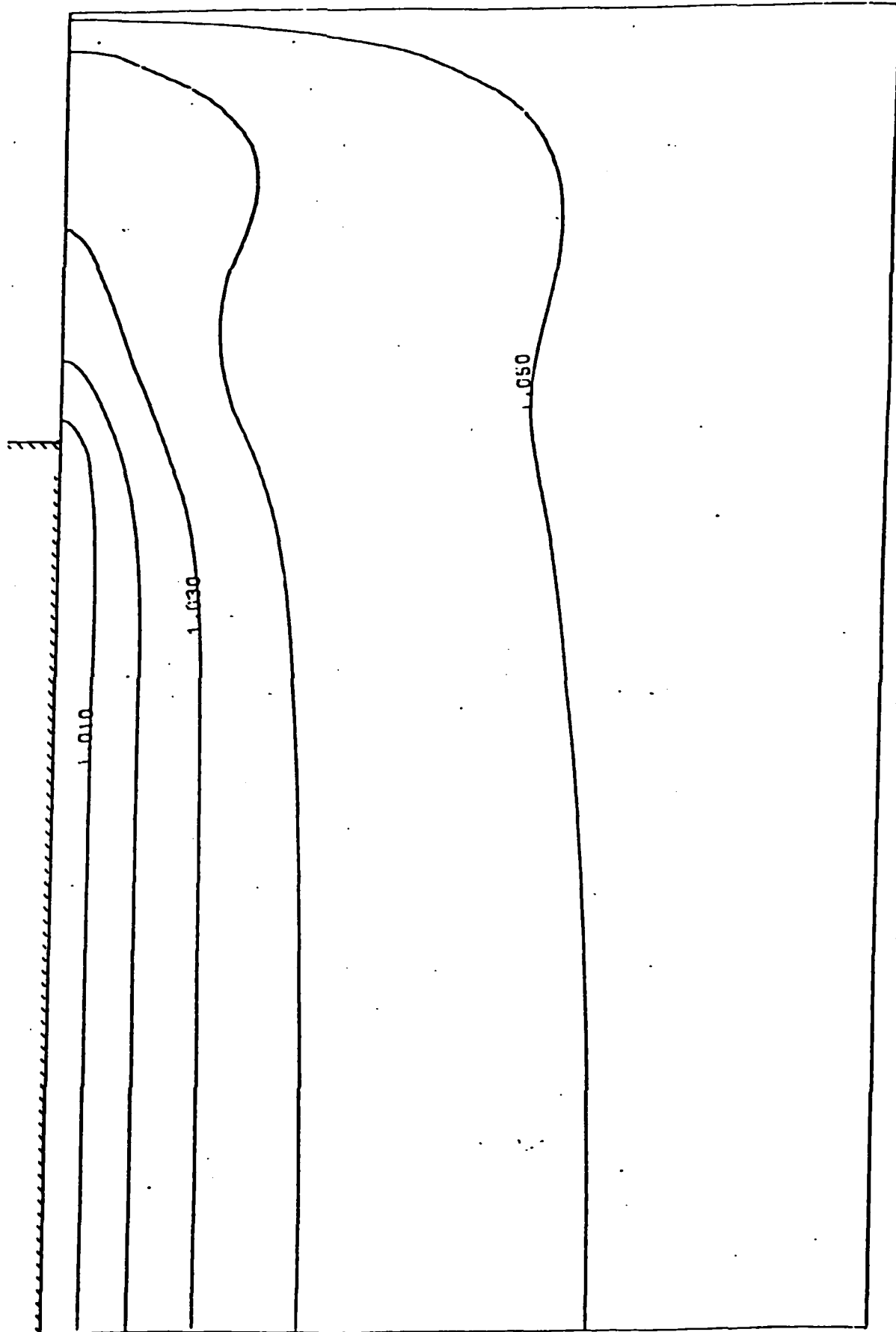


Fig. 4 - Temperature contours. Stationary crucible case.

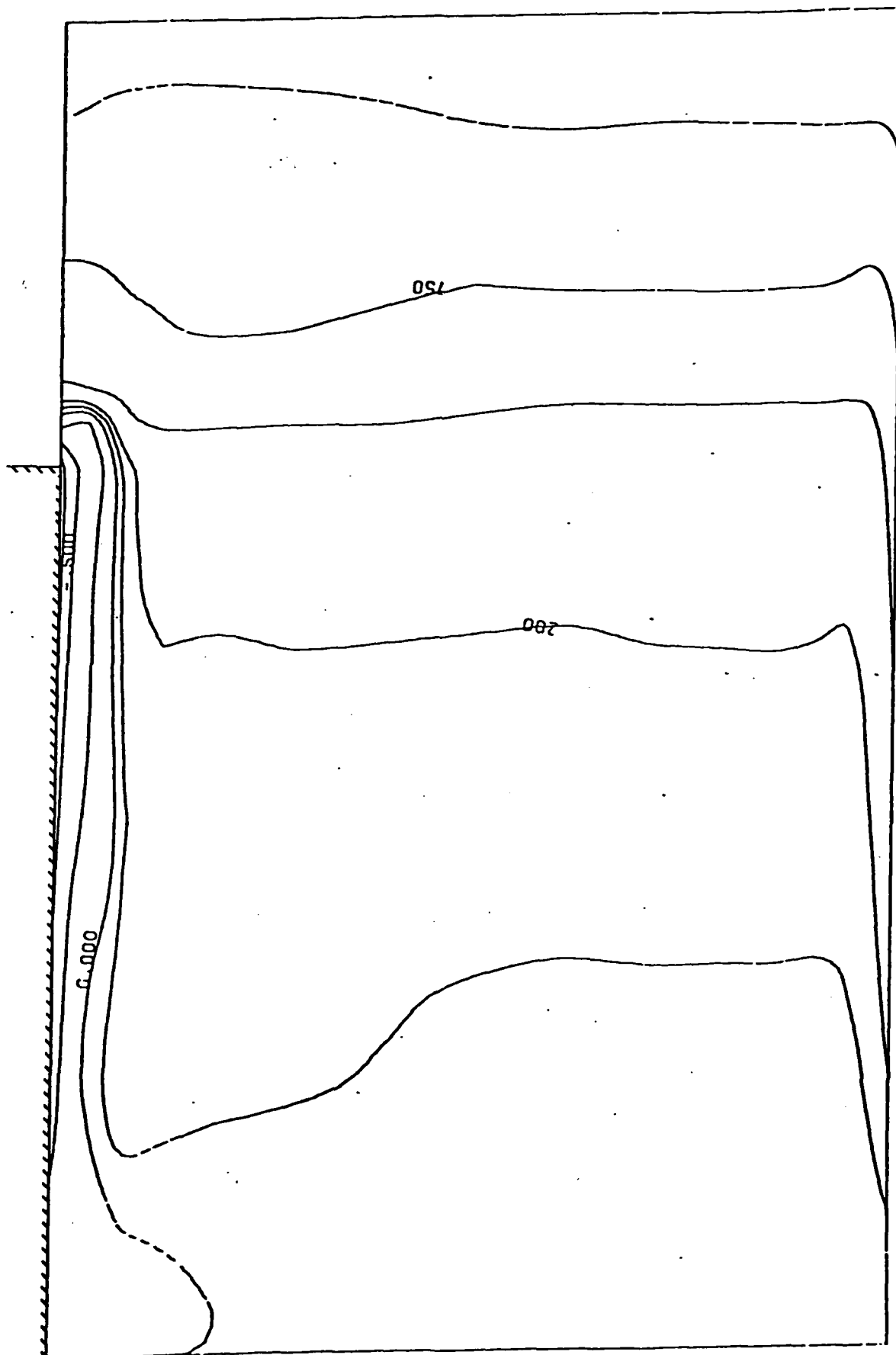


Fig. 5 - Azimuthal velocity contours, rotating crucible case.
Contour levels at $-.9$, $-.5$, $-.2$, 0 , $.1$, $.2$, $.5$, $.75$, $.9$.

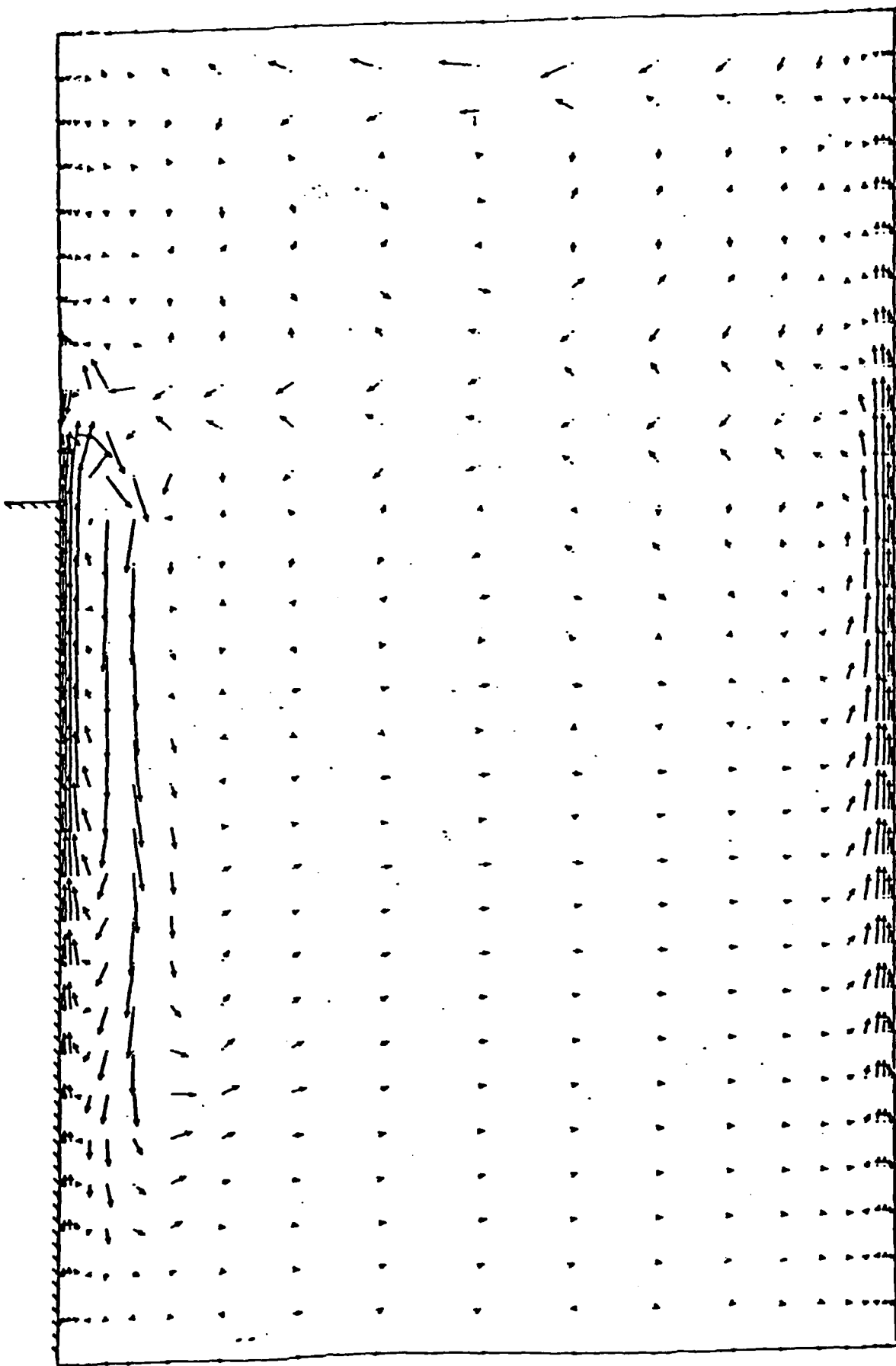


Fig. 6 - Secondary flow, rotating crucible case.

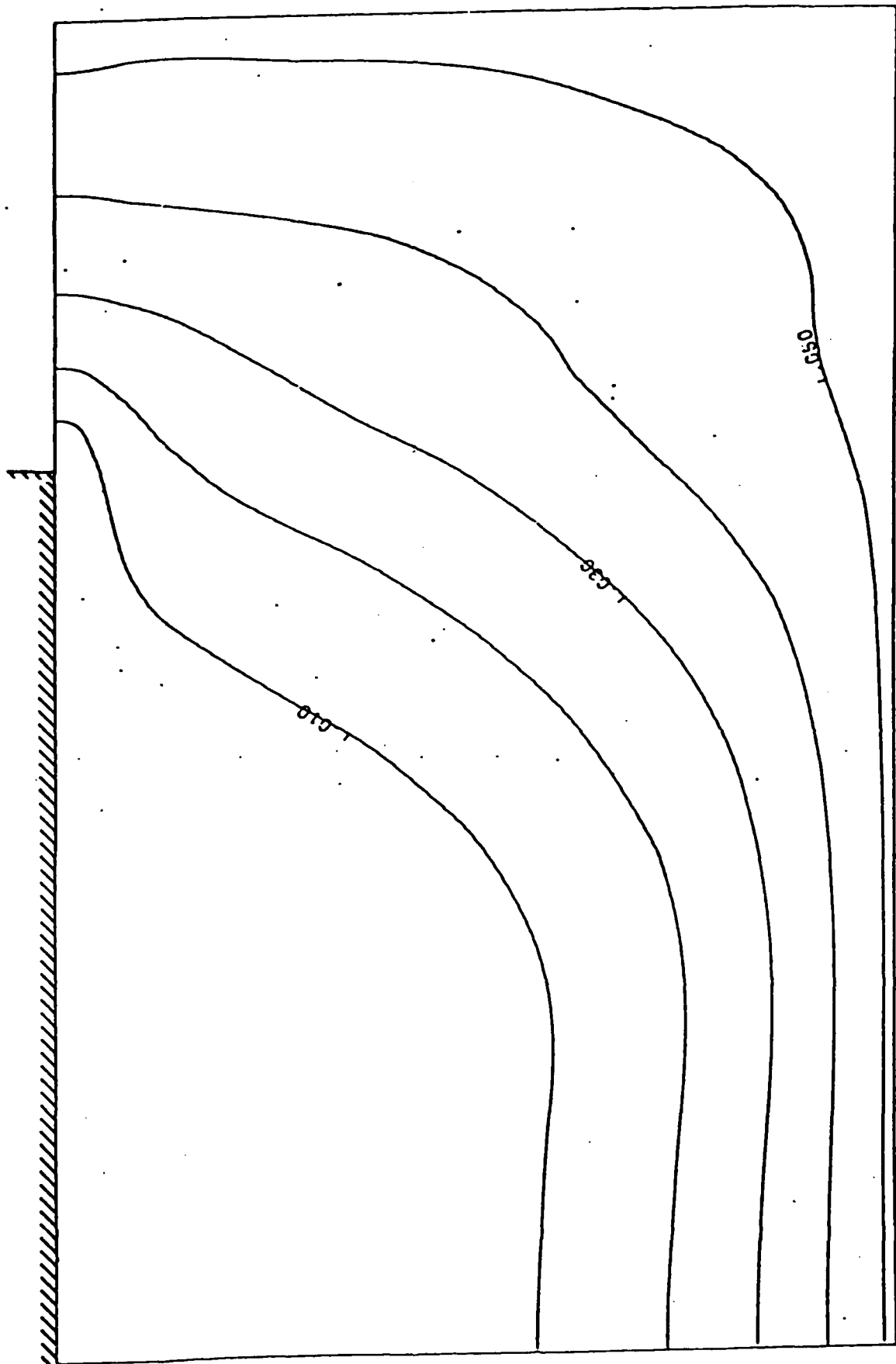


Fig. 7 - Temperature contours, rotating crucible case.

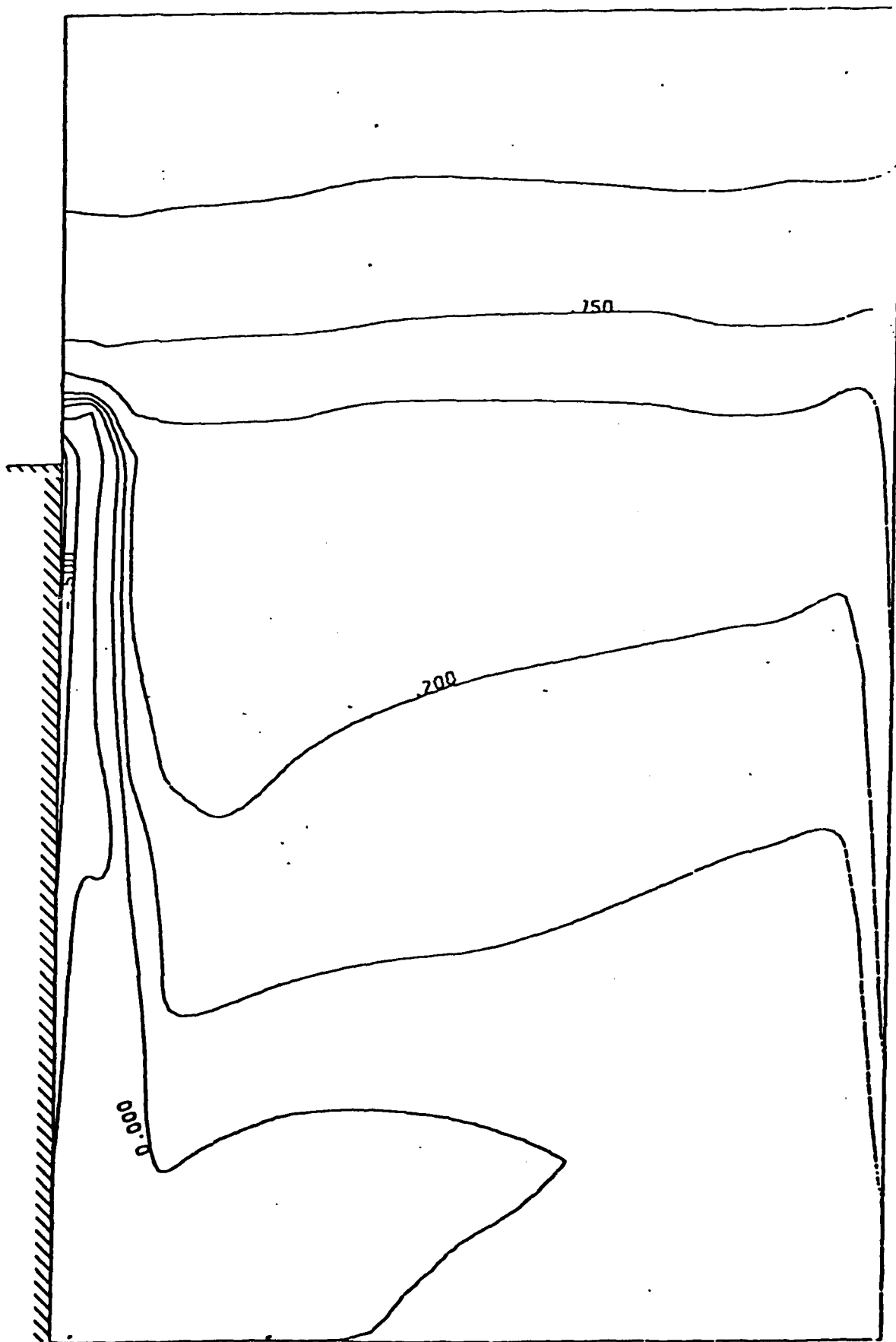


Fig. 8 - Azimuthal velocity contours, rotating crucible with buoyancy.
Contour levels at -.8, -.5, -.2, 0, .1, .2, .5, .75, .9.

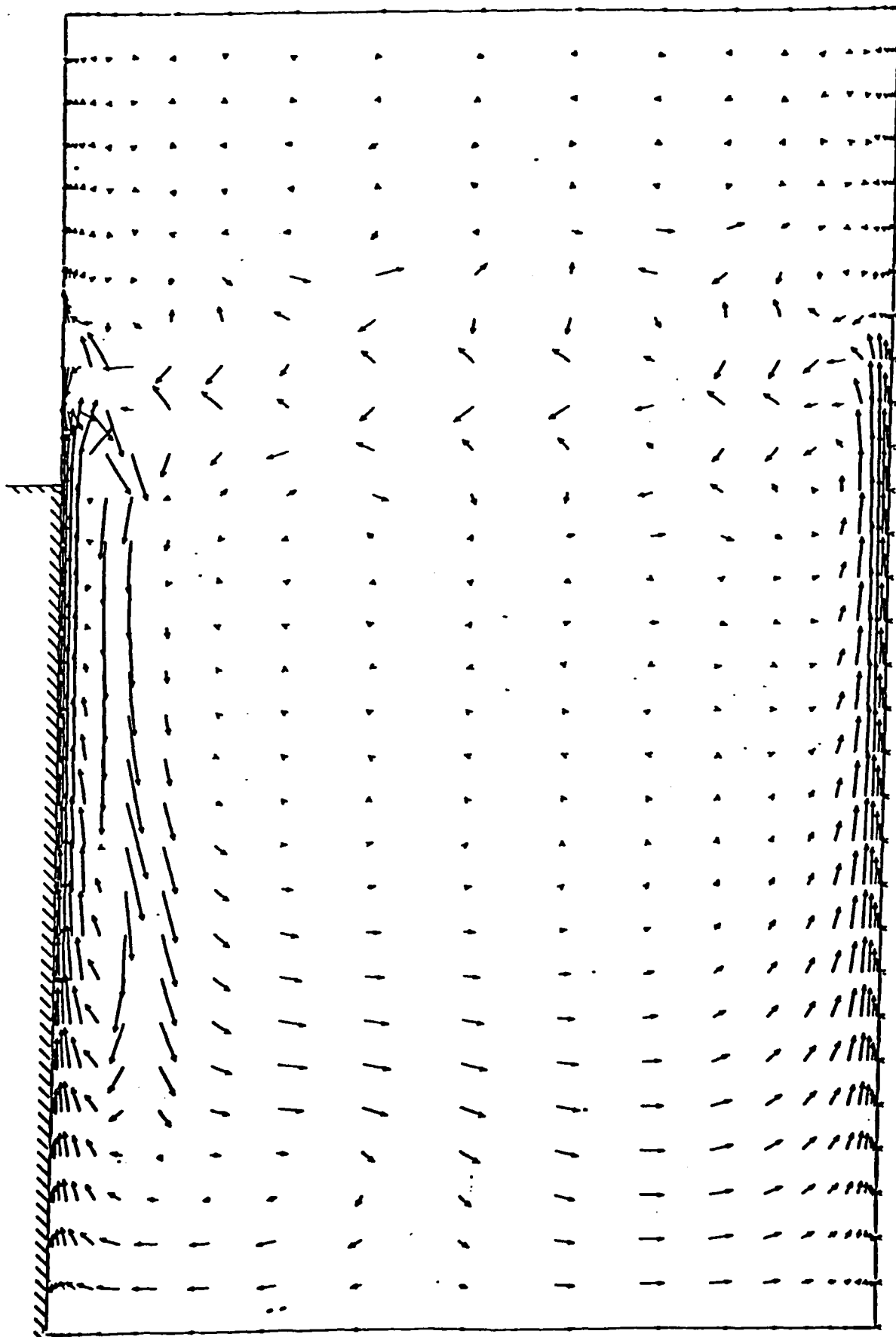


Fig. 9 - Secondary flow, rotating crucible with buoyancy.

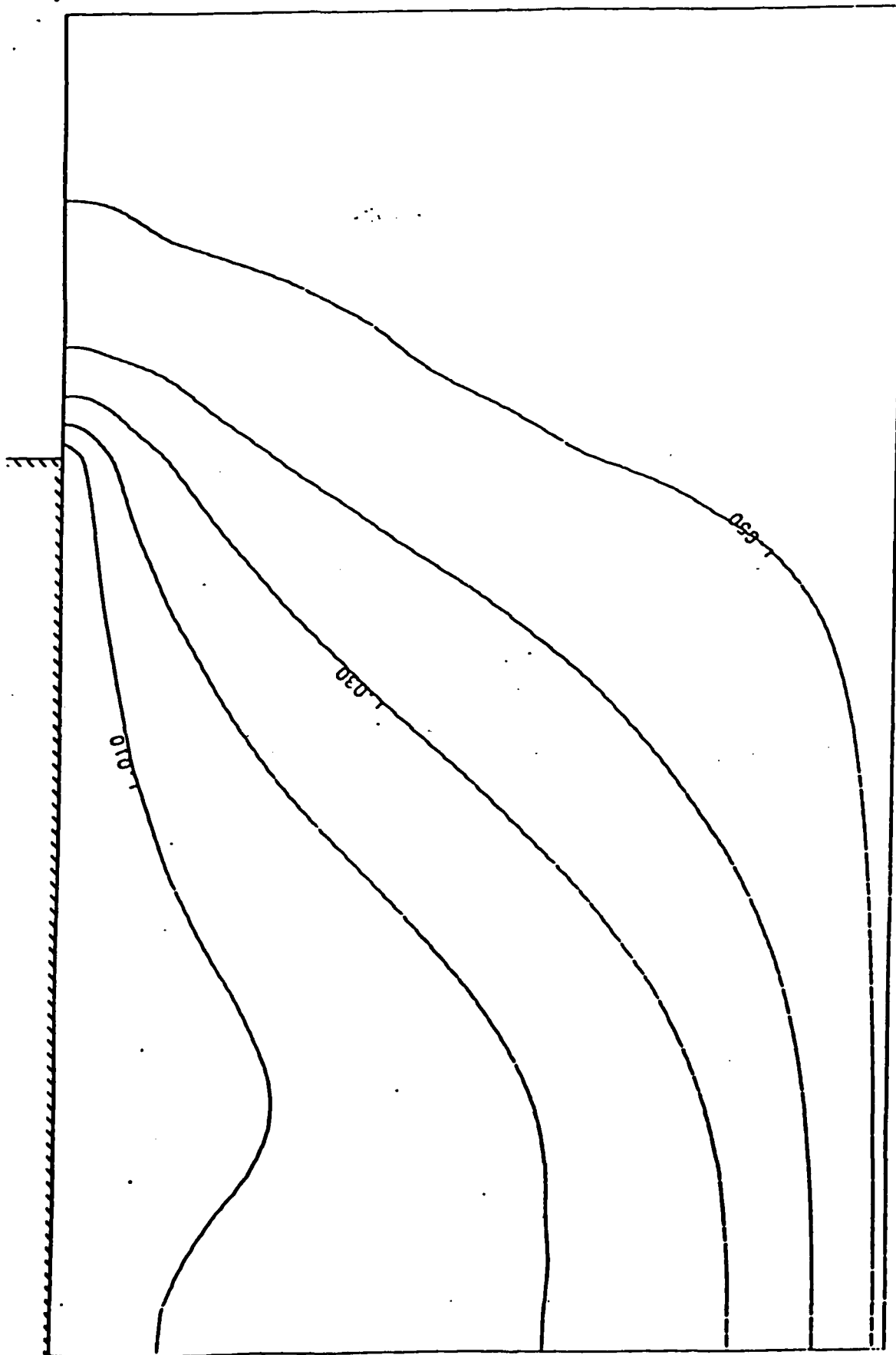


Fig. 10 - Temperature contours, rotating crucible with buoyancy.

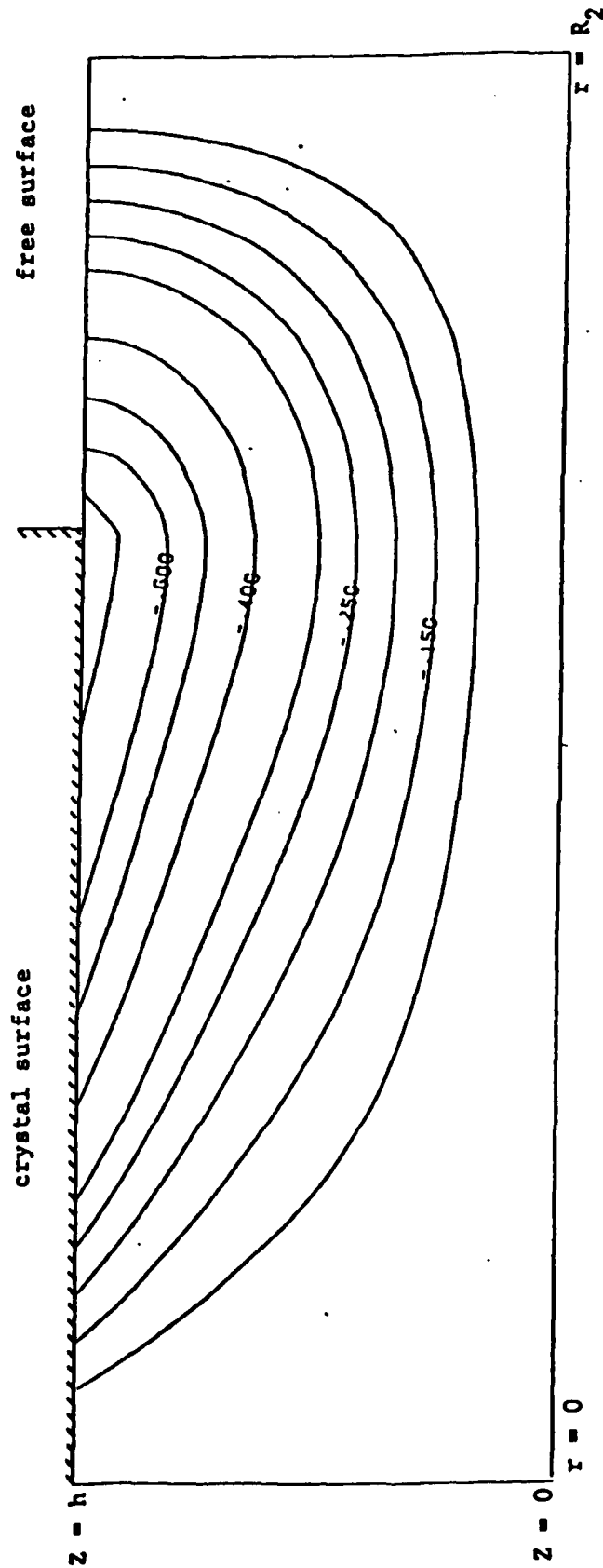


Fig. 11 - Azimuthal velocity contours, stationary crucible case (low Reynolds number contour levels at -.8, -.6, -.5, -.4, -.3, -.25, -.2, -.15, -.1).

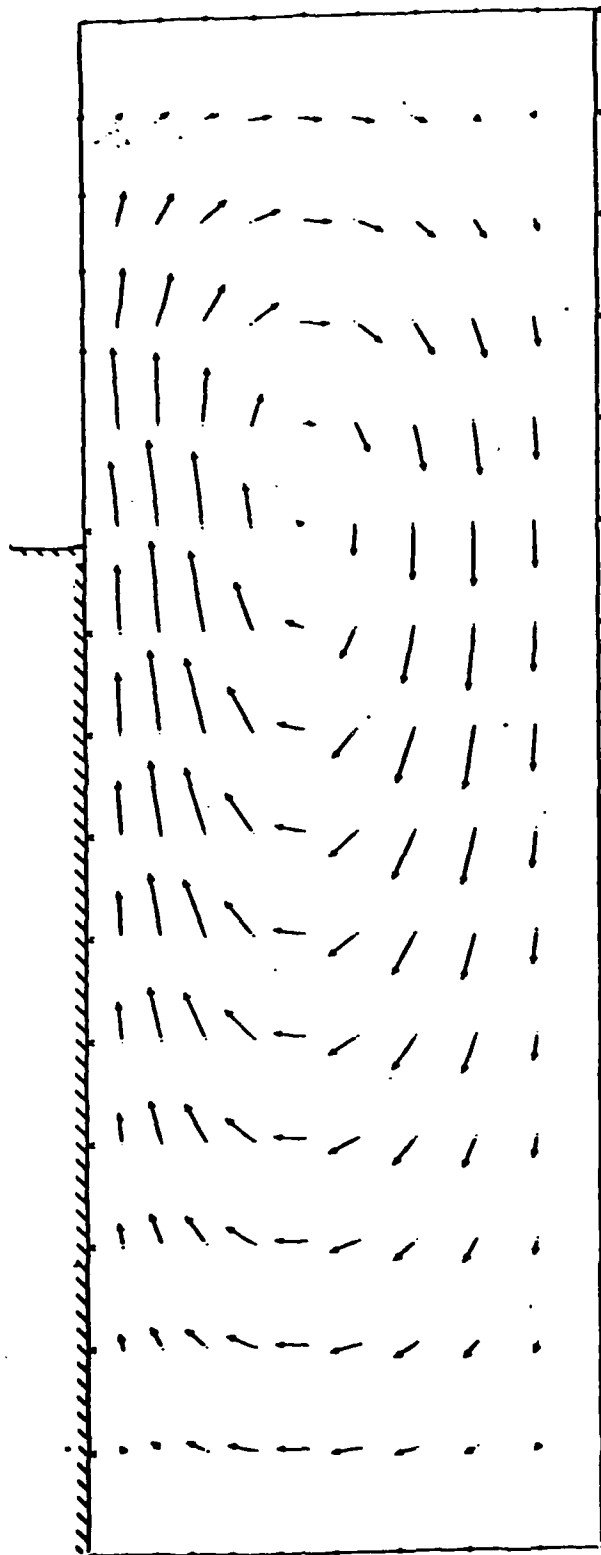


Fig. 12 - Secondary flow, stationary crucible case (low Reynolds number).

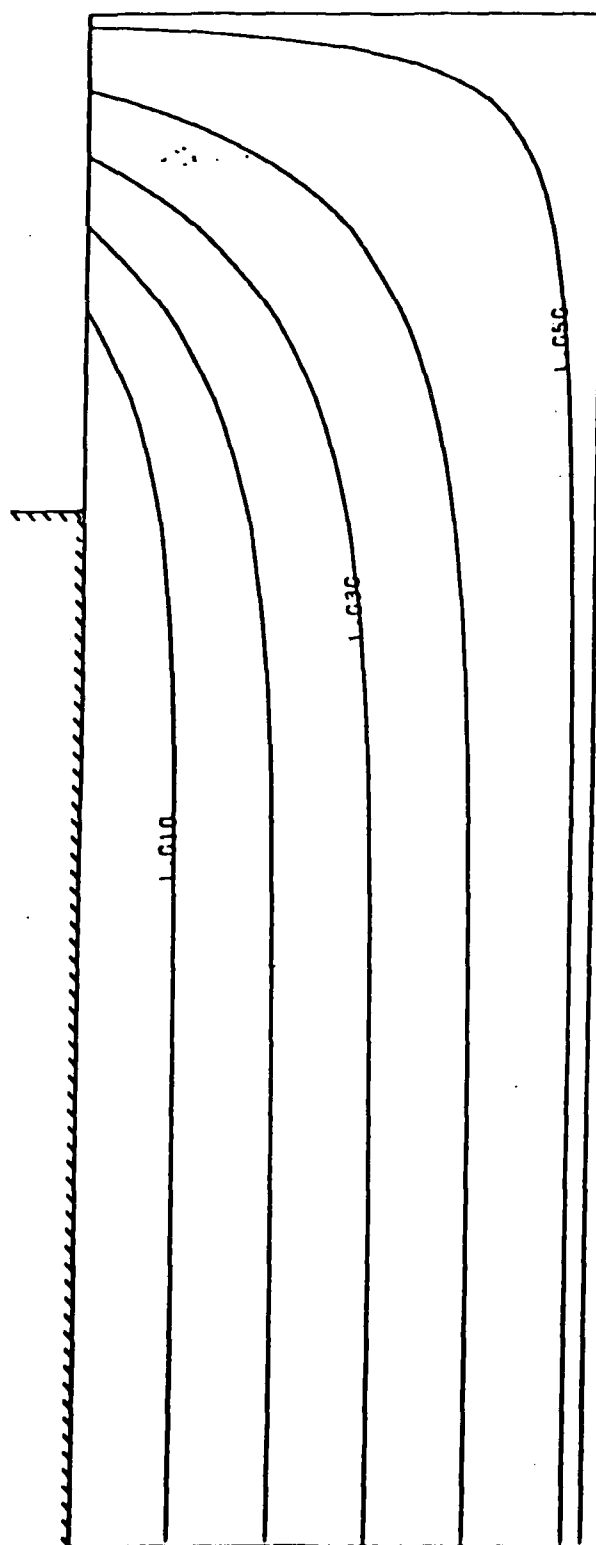


Fig. 13 - Temperature contours, stationary crucible case (low Reynolds number).

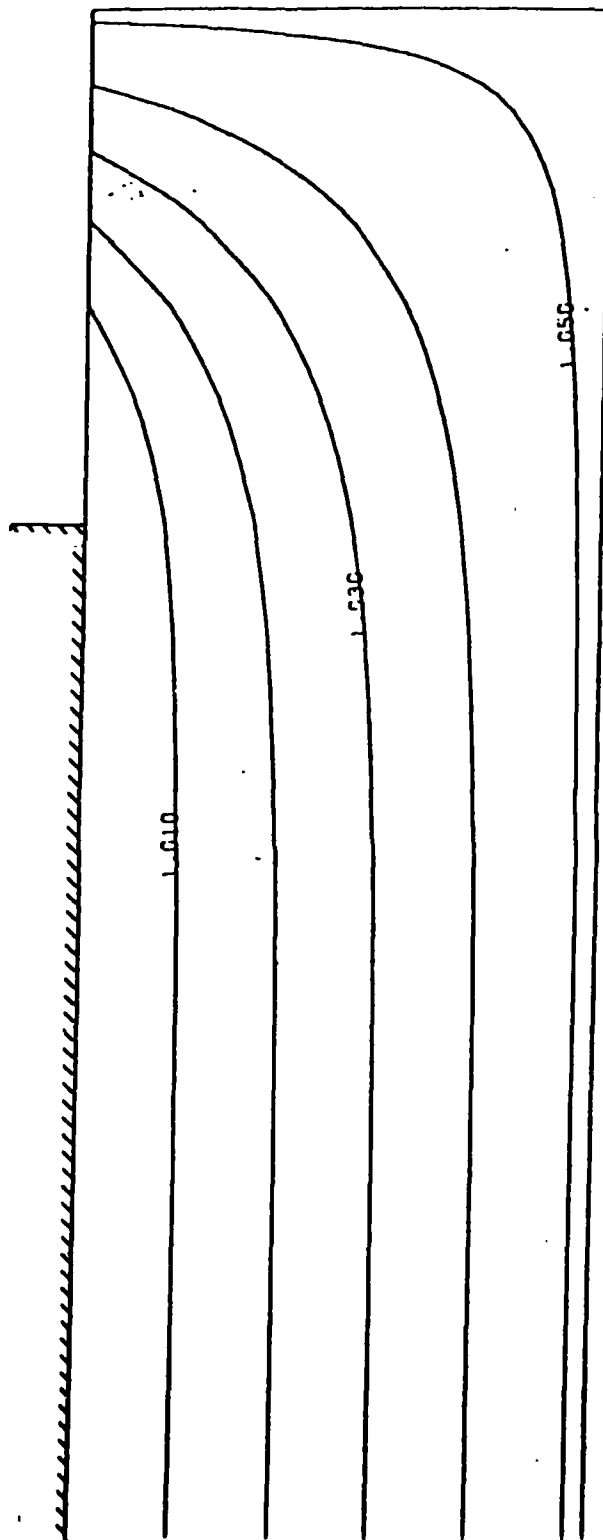


Fig. 14 - Temperature contours at $\theta = 36^\circ$, three-dimensional case (hot spot).
Contour levels at 1.00, 1.01, 1.02, 1.03, 1.04, 1.05, 1.06, 1.07, 1.08.

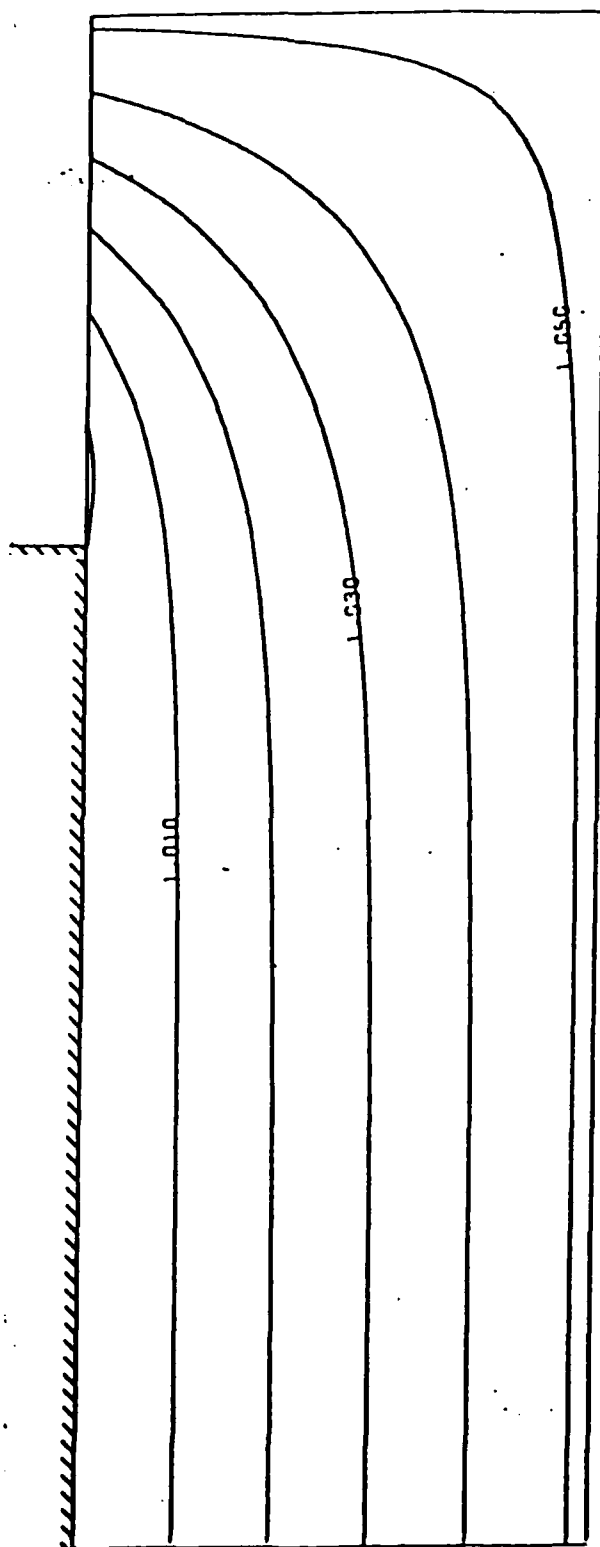


Fig. 15 - Temperature contours at $\theta = 60^\circ$, three-dimensional case (hot speed).
Contour levels at 1.00, 1.01, 1.02, 1.03, 1.04, 1.05, 1.06, 1.07, 1.08.

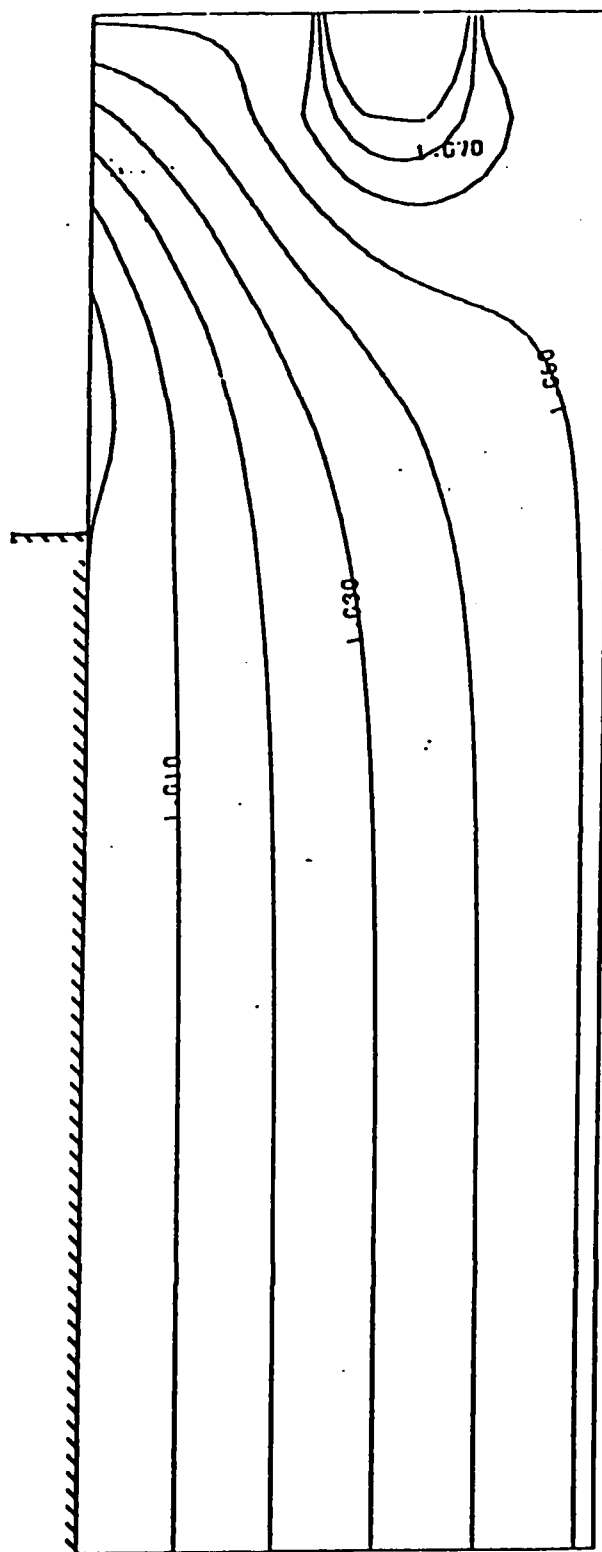


Fig. 16 - Temperature contours at $\theta = 84^\circ$, three-dimensional case (hot spot).
Contour levels at 1.00, 1.01, 1.02, 1.03, 1.04, 1.05, 1.06, 1.07, 1.08.

A LOW MACH NUMBER FORMULATION OF THE
COMPRESSIBLE EULER EQUATIONS

W. R. Briley, H. McDonald and S. J. Shamroth
Scientific Research Associates, Inc.
Glastonbury, CT 06033

SRA Report 82-1

ABSTRACT

It is well known that flow of a perfect gas at low Mach number closely approximates an incompressible flow, provided there is no heat addition. The usual formulation of the compressible Euler equations encounters singular behavior as the Mach number approaches zero. The Euler equations for a perfect gas are written here in variables which are well behaved for adiabatic flow at low Mach number and in a form which reduces to the incompressible (constant density) Euler equations as the Mach number approaches zero. The present formulation clarifies how the reduction to incompressible flow occurs and is useful in constructing numerical algorithms for low Mach number and other flows.

BACKGROUND

Incompressible Euler Equations

The incompressible Euler Equations can be expressed in nondimensional vector form as

$$\nabla \cdot \bar{U} = 0 \quad (1)$$

$$\frac{\partial \bar{U}}{\partial t} + (\bar{U} \cdot \nabla) \bar{U} + \nabla \left(\frac{c_p}{2} \right) = 0 \quad (2)$$

where \bar{U} is the velocity vector, c_p is a pressure coefficient, and t is time.

The pressure coefficient is defined by

$$c_p = 2 (p - P_1) \quad (3)$$

where p is pressure and P_1 is an arbitrary (constant) pressure basis. Here (and subsequently), all variables are nondimensional, having been normalized by reference quantities denoted by a subscript 'r'. The reference pressure p_r has been taken as $\rho_r U_r^2$, where ρ denotes density.

The continuity equation (1) and the three components of momentum (2) comprise four equations governing c_p (or equivalently p) and the three components of \bar{U} . For incompressible flow, c_p and \bar{U} are independent of the temperature T , which in turn is governed by an energy equation that does depend on \bar{U} .

Compressible Euler Equations

The compressible continuity and momentum equations can be written in the following form:

$$\frac{\partial (\ln \rho)}{\partial t} + \nabla \cdot \bar{U} + \bar{U} \cdot \nabla (\ln \rho) = 0 \quad (4)$$

$$\frac{\partial \bar{U}}{\partial t} + \bar{U} \frac{\partial (\ln \rho)}{\partial t} + (\bar{U} \cdot \nabla) \bar{U} + \nabla \left(\frac{p}{\rho} \right) + \frac{p}{\rho} \nabla (\ln \rho) = 0 \quad (5)$$

The equation of state for a perfect gas can be expressed as

$$P = \rho T / \gamma M^2 \quad (6)$$

where γ is the specific heat ratio, and the reference Mach number M is given by $M = U_r / c$. Here, c is the reference speed of sound defined by $c^2 = \gamma R T_r$, and R is the gas constant. The 'r' subscript on M is omitted for convenience, but no confusion should arise since only the reference Mach number will be referred to subsequently. The system is closed by the energy equation, which may be

written as

$$\frac{\partial T}{\partial t} + \bar{U} \cdot \nabla T = (\gamma - 1) T \nabla \cdot \bar{U} \quad (7)$$

The usual method of reducing the compressible equations to the incompressible equations is to assume a constant density and note that an equation of state is no longer needed. As a limiting process, however, the equation of state (6) indicates that p becomes infinite as $M \rightarrow 0$ (unless $T \rightarrow 0$). Equations (4 - 7) are reformulated here as a system of equations which remains well behaved as $M \rightarrow 0$.

LOW MACH NUMBER FORMULATION

To relate the compressible and incompressible equations, a new dependent variable \hat{c}_p relating p and ρ is introduced and defined by

$$\hat{c}_p \equiv \frac{2}{\gamma M^2} \frac{1}{\rho} (\gamma M^2 p - P_2) \quad (8)$$

where P_2 is an arbitrary (constant) pressure basis. Using Eq. (8) to eliminate p in the momentum equation (5) leads to

$$\frac{\partial \bar{U}}{\partial t} + \bar{U} \frac{\partial (\ln \rho)}{\partial t} + (\bar{U} \cdot \nabla) \bar{U} + \nabla \cdot \frac{\hat{c}_p}{2} + \frac{\hat{c}_p}{2} \nabla (\ln \rho) = 0 \quad (9)$$

The definition of (nondimensional) stagnation enthalpy E is

$$E = T + (\gamma - 1) M^2 q^2 / 2 \quad (10)$$

where $q^2 \equiv \bar{U} \cdot \bar{U}$, and E_r has been taken as $C_p T_r$, where C_p is the specific heat at constant pressure. Combining the equation of state (6) and the definition of stagnation enthalpy (10) gives

$$p = \rho [E / \gamma M^2 - (\gamma - 1) q^2 / 2\gamma] \quad (11)$$

Combining Eqs. (8) and (11) to eliminate p leads to

$$\rho = P_2 [E - \frac{\gamma M^2}{2} \hat{c}_p - \frac{(\gamma - 1) M^2}{2} q^2]^{-1} \quad (12)$$

For a wide range of flow conditions, including adiabatic flow at low Mach number, the stagnation enthalpy E may be assumed to be a known constant. In this instance, Eq. (12) relates ρ , \hat{c}_p , and \bar{U} and serves to decouple the continuity and momentum equations (4) and (9) from the energy equation (7), which can be omitted from consideration. The system of governing equations then consists of Eqs. (4), (9), and (12), with dependent variables ρ , \hat{c}_p , and \bar{U} .

Note from Eq. (12) that $\rho \rightarrow P_2/E$ (a constant) as $M \rightarrow 0$. As a consequence, the terms containing $\nabla(\ln \rho)$ in Eqs. (4) and (9) vanish as $M \rightarrow 0$, and these equations thus reduce to the incompressible form of Eqs. (1) and (2). The limit $M \rightarrow 0$ is taken by letting $R \rightarrow \infty$, which allows $U_r, \rho_r, T_r, \gamma = O(1)$.

In this formulation,

$$\hat{c}_p \rightarrow c_p, \rho \rightarrow 1 \text{ as } M \rightarrow 0 \quad (13)$$

assuming appropriate choices are made for P_1, P_2 , and E . To guide these choices, it is noted that selecting $P_2 = 1, E = 1 + (\gamma-1)M^2/2$ implies that $\hat{c}_p = 0$ and $\rho = T = 1$ where $q = 1$ (freestream basis condition for P_1). The choice $P_2 = E = 1$ implies that $\hat{c}_p = 0$ and $\rho = T = 1$ where $q = 0$ (stagnation-point basis for P_1). With either choice for P_2 and E , $\hat{c}_p \rightarrow c_p$ follows as $M \rightarrow 0$ because \hat{c}_p and c_p satisfy the same governing equations and boundary conditions and are equal at the basis point. Also, since $\rho \rightarrow 1$ as $M \rightarrow 0$, $\ln \rho$ itself approaches zero as $M \rightarrow 0$.

It is important to distinguish the roles played by \hat{c}_p and by the assumption of constant E . The change of variables from p to \hat{c}_p is responsible for eliminating the singular behavior which would otherwise occur in Eq. (11) whether or not E is constant. The assumption of constant stagnation enthalpy is not a requirement for use of the low Mach number formulation of the equations, and is necessary only if the compressible equations are to imply constant density as $M \rightarrow 0$ (cf. Eq. 12). It is thus clear that the physical motivation for requiring constant stagnation enthalpy at low Mach number is to produce a flow field with nearly constant density.

It is also worth noting that since $\nabla \cdot \bar{U} \rightarrow 0$ as $M \rightarrow 0$, the last term in the energy equation (7) vanishes, and this equation thus reduces to its incompressible form

$$\frac{\partial T}{\partial t} + \bar{U} \cdot \nabla T = 0 \quad (14)$$

Since Eqs. (10) and (12) imply that $T \rightarrow E$ and $\rho \rightarrow P_2/E$ as $M \rightarrow 0$, it is evident that taking E as constant as $M \rightarrow 0$ does not permit a variable T , and if E varies, then ρ varies as T^{-1} . Nevertheless, the present formulation can be used to treat incompressible (constant density) flows with nonconstant temperature by taking E as constant and omitting Eq. (10). This can be justified by noting that for small Mach number (say $M < 0.1$) and constant E , the present system for a perfect gas closely approximates a constant density incompressible flow and is thus a good model (for example) for flow of a liquid whose (constant) density is assumed to be

independent of temperature. In this instance, the quantity E in Eq. (12) is reinterpreted as a nonphysical modeling parameter which serves to decouple the continuity and momentum equations from the energy equation, as required for the liquid. The incompressible energy equation (14) can then be solved separately for the physical temperature variation, and the incompressible constant-density liquid is thus modeled as a very slightly compressible fluid with constant 'stagnation enthalpy'. The Boussinesq assumption for natural convection can be introduced within this same context by adding a body force term (which depends only on temperature) to the momentum equation.

As a separate issue, it is worth noting that the assumption of constant stagnation enthalpy is useful over a wide range of flow conditions and is much more general than is an assumption of isentropic flow. The constant stagnation enthalpy assumption is reasonable for transonic and supersonic flow with shocks and also for adiabatic viscous flow with unit Prandtl number and no viscous heating. The authors have made extensive use of this assumption in treating viscous flow at supersonic, low subsonic, and transonic Mach numbers (eg. Refs. 1-3).

REFERENCES

1. McDonald, H. and Briley, W.R.: Three-Dimensional Supersonic Flow of a Viscous or Inviscid Gas, Journal of Computational Physics, Vol. 19, 1975, pp. 150 - 178.
2. Briley, W.R. and McDonald, H.: Computation of Three-Dimensional Horseshoe Vortex Flow Using the Navier-Stokes Equations, Seventh International Conference on Numerical Methods in Fluid Dynamics, Proceedings, Stanford 1980, Springer-Verlag, pp. 91 - 98.
3. Shamroth, S.J., McDonald, H. and Briley, W.R.: Application of Navier-Stokes Analysis to Transonic Cascade Flow Fields, ASME Paper 82-GT-235, 1982.

DATE
FILMED
1968